

Journal of Seismic Exploration

ARTICLE

A novel wavefield reconstruction inversion method using an approximated model-domain Hessian

Huaishan Liu^{1,2,3}, Yuzhao Lin³, Lei Xing³, Jinghao Li³, Kun Huang³ and Hehao Tang³

¹State Key Laboratory of Shale Oil and Gas Enrichment Mechanisms and Efficient Development, Beijing, China

²Key Laboratory of Oil & Gas Reservoir Geophysics, Sinopec, Beijing, China

³Department of Marine Geophysics, College of Marine Geosciences, Ocean University of China, Qingdao, Shandong, China

Abstract

The Hessian matrix, though computationally expensive, plays a critical role in ensuring inversion accuracy and mitigating cross-talk in multi-parameter inversion. The well-known wavefield reconstruction inversion (WRI) or extended space full-waveform inversion can reduce nonlinearity and mitigate cycle skipping in traditional FWI. However, most implementations omit the Hessian. In this study, the Hessian—formulated as a function of measurement and theoretical covariance matrices—is incorporated into WRI within a Bayesian inference framework. Furthermore, the connections between the data- and model-domain Hessian equations are discussed, leading to a simplified calculation method for the extended source. Based on this approach, a new definition for the theoretical covariance matrix is proposed and validated through numerical tests, demonstrating its accuracy.

Keywords: Inversion; Bayesian inference; Theory covariance matrix

*Corresponding author: Yuzhao Lin (linyuzhao@ouc.edu.cn)

Citation: Liu H, Lin Y, Xing L, Li J, Huang K, Tang H. A novel wavefield reconstruction inversion method using an approximated modeldomain Hessian. *J Seismic Explor*. doi: 10.36922/JSE025250018

Received: June 16, 2025 Revised: August 15, 2025 Accepted: September 3, 2025 Published online: November 3, 2025

Copyright: © 2025 Author(s). This is an Open-Access article distributed under the terms of the Creative Commons Attribution License, permitting distribution, and reproduction in any medium, provided the original work is properly cited.

Publisher's Note: AccScience Publishing remains neutral with regard to jurisdictional claims in published maps and institutional affiliations.

1. Introduction

Full-waveform inversion (FWI),^{1,2} a tool commonly used to invert subsurface structures, has been widely used in geophysics exploration.^{3,4} However, as a data-fitting algorithm in the least squares sense, FWI suffers from cycle skipping and nonlinearity, primarily due to the difficulty of predicting the data resulting from the inexpressive wave equation and the limited acquisition aperture.⁵

There are methods specifically designed to address cycle skipping, which generally involves a complex operation for each trace^{6,7} or shot⁸ to achieve accurate matching. An advanced method for measuring distance using optimal transport distances has garnered the attention of a wide range of researchers and has been well-developed.⁹⁻¹² As for nonlinearity, the multi-scale strategy,^{12,13} changing the inversion domain,¹⁴ or modifying the objective function form¹⁵ can help alleviate this limitation.

In addition to the above methods, two other directions have been proposed and developed into relatively mature methods. One is an extended space FWI (ES-FWI), which introduces another search space in the inversion.

There are two ways to build the ES-FWI method. The first approach is to add non-physical degrees of freedom to the model, thereby pushing the synthetic data to better fit the observed data.¹⁶ However, new space introduces additional computational costs through either increased calculation time for the new forward operator or more storage requirements for new variables. Various methods have been proposed to reduce computational cost,^{17,18} in which the extended source FWI¹⁹ is a more efficient method, as it only inverts the extended source and the model parameters. A study by Symes²⁰ provided a detailed analysis of why the extended source FWI is effective.

The other method is the wavefield reconstruction inversion (WRI), which starts by incorporating the wave equation into the objective function to reduce nonlinearity and computational cost.²¹ Leeuwen and Herrmann²² conducted a more mathematical analysis of the proposed method and carefully analyzed the selection strategy of the penalty scalar.²² However, it was initially proposed in the frequency domain, requiring an augmented wave equation that is challenging to solve in the time domain. In addition, the physical meaning of certain variables (reconstructed wavefield, penalty scalar) and the tuning method for the penalty scalar when solving WRI require clarification.

Several studies have been conducted to address the above challenge, including rough approximations that enable WRI in the time domain, 23,24 resulting in more precise solutions proposed. Rizzuti et al.25 proposed a data-dual formulation of WRI, where the Lagrange formula is used to reformulate the WRI, making it easier to apply to large three-dimensional models in the time domain.^{25,26} Moreover, the iterative refining-WRI method was proposed, in which an enhanced Lagrange method equipped with operator splitting is used instead of the penalty method, with its regularization and corresponding expansion in other media investigated accordingly.²⁷⁻²⁹ For the adjustment of the penalty scalar, a rough local optimization method was used.30 Gholami et al.31 treated the penalty scalar as a variable that needs to be inverted. In addition, Gholami et al. 32 discussed the physical meaning of the reconstructed wavefield, while Lin et al. 33 elucidated the mechanism of low-wavenumber update in WRI.

In general, although both extended FWI and WRI are essentially ES-FWI, there are apparent differences between them. Extended FWI expands space by introducing

seismic-related variables (e.g., offset, wavelet) into model space, while WRI uses model space in the sense of the wavefield. Extended FWI utilizes the introduced space or variables to achieve an accurate data fit, while WRI reduces the impact of non-linearity and non-physical data through wavefield matching. However, both methods require delicate settings of the inversion parameters. Operto *et al.*³⁴ reviewed the above ES-FWI methods within the framework of inverse scattering theory, in which the Lippmann–Schwinger equation was used to govern modeling.³⁴ In addition to ES-FWI, the Hessian is typically used to ensure inversion accuracy in traditional FWI. However, computing the Hessian remains challenging due to its large scale. Furthermore, the Hessian is commonly not included in WRI or ES-FWI.

In this paper, we analyze these inversion methods using the Bayesian inference theory. Notably, all inversion methods can be formulated uniformly using Bayesian inference theory, which can bring substantial advantages.^{3,35} First, deriving inversion methods from Bayesian inference can provide a more accurate representation of the problem. Figueiredo *et al.*³⁶ and Huang *et al.*³⁷ used the Bayesian theory to develop a more precise inversion method for an anisotropic medium.^{36,37} Furthermore, a reduced nonlinear inversion can be obtained. Moreover, Leeuwen³⁸ and Lin *et al.*³⁹ re-derived WRI from Bayesian inference and accelerated the inversion by redefining the theoretical covariance matrix.^{38,39}

The main contribution of this paper is a simplified theoretical definition of the covariance matrix to alleviate the computational problem of WRI. This paper is organized as follows: first, the WRI is re-derived from Bayesian inference to illustrate how the statistical variables included in the model or data domain Hessian affect or improve the inversion methods. Next, by comparing the data and model domain methods, we provide a simplified extended source calculation method. Finally, corresponding numerical tests are shown to demonstrate the effectiveness of different theoretical covariance matrix definitions.

2. Theory

2.1. Seismic inversion based on Bayesian inference

Various ES-FWI methods have been developed for different concerns. In this section, we derive the original WRI from Bayesian inference, in which the Hessian is naturally introduced. First, the wavefield term u is introduced into the Bayesian inference (**Equation I**):³⁹

$$\rho_{post}(u, m|d) \propto \rho_{like}(d|m, u) \rho_{prior}(u, m)$$
(I)

Where the likelihood of probability density function is:

$$\rho_{like} (d|m, u) = exp - \frac{1}{2} (d - Pu)^* \Sigma_{obs}^{-1} (d - Pu) + exp - \frac{1}{2} (q - Au)^* \Sigma_{syn}^{-1} (q - Au)$$
(II)

in which m denotes the interested model parameters, d represents the observed data, P is the sampling operator, u denotes the seismic source, A is the forward operator, and Σ_{obs} , Σ_{sym} are the measurement and theoretical covariance matrices, respectively (**Equation II**). ρ_{prior} denotes the prior knowledge of the wavefield and model parameters, which will be excluded in this paper to simplify the calculation. Maximizing the posterior leads to the following minimization problem:

$$\phi(m, u) = (d - Pu)^* \sum_{obs}^{-1} (d - Pu) + (q - A(m)u)^* \sum_{syn}^{-1} (q - A(m)u)$$
(III)

There are two ways to solve **Equation III**, which will be discussed in the following section.

2.2. WRI based on the data-domain Hessian

We assumed the measurement uncertainty is random, and the measurement covariance matrix is $\Sigma_{obs}^{-1} = \lambda_{obs} I$. Then, by keeping the model m fixed and setting the derivative of **Equation III** with respect to the wavefield to zero, we obtain **Equation IV**:

$$A\hat{u} = q + \lambda_{obs} \Sigma_{syn} A^{-*} P^* \delta d \tag{IV}$$

Where $\delta d = d - P\hat{u}$ and \hat{u} denotes the reconstructed wavefield. The reconstructed wavefield on both sides makes the above equation challenging to solve, and moving the reconstructed wavefield to one side is difficult to perform due to the complex combination of the forward operators. Approximate or alternative measurements have been proposed by Lin *et al.*¹² to address these challenges.¹² Essentially, the above equation involves the data-domain Hessian, where δd can be solved by **Equation V**:

$$H_d \, \delta d = \delta d^0 \tag{V}$$

where $\delta d^0 = d - Pu$, u is the background or current wavefield, and

$$H_d = \lambda_{obs} (PA^{-1}) \Sigma_{syn} (PA^{-1})^* + I$$
 (VI)

as in Gholami et al.40 (Equation VI).

With the reconstructed wavefield, \hat{u} we can obtain an update for the model parameters by calculating the derivative of the objective function with respect to

the model, and replacing the latter term according to **Equation IV**, we have **Equation VII**:

$$g = -\left(\frac{\partial A\hat{u}}{\partial m}\right)^* \Sigma_{syn}^{-1} (A\hat{u} - q) = -\lambda_{obs} \left(\frac{\partial A\hat{u}}{\partial m}\right)^* A^{-*} P^* \delta d$$
 (VII)

The gradient is a zero-lag correlation between the reconstructed wavefield and the back-propagated residual blurred by the data-domain Hessian with the theoretical covariance matrix. The calculation of the data-domain Hessian is computationally infeasible due to its large scale. Lin *et al.*³⁹ proposed a point spread function-based method to alleviate this challenge. Furthermore, a proper theoretical covariance matrix definition has been proven to be another way to mitigate the computational problem.³⁹

2.3. WRI based on the model-domain Hessian

Clearly, the data-domain Hessian is challenging to compute; however, it remains essential for achieving accurate WRI. An alternative is to reformulate the problem in a different domain. By starting with the data-domain Hessian and the weighted residual in WRI and FWRI, and multiplying $(PA^{-1})^*$ on both sides of **Equation V**, we transform it into the model-domain equation (**Equation VIII**):

$$[\lambda_{obs}(PA^{-1})^*(PA^{-1})\Sigma_{syn} + I]\hat{s} = s_0$$
 (VIII)

where $\hat{s} = (PA^{-1})^* \delta d$, $s_0 = \lambda_{obs} (PA^{-1})^* \delta d^0$, similar to the adjoint state definitions.⁴¹ In this case, instead of inverting the data-domain Hessian, we consider the inversion of the model-domain Hessian (**Equation IX**):

$$H_m = \lambda_{obs} (PA^{-1})^* (PA^{-1}) \Sigma_{syn} + I$$
 (IX)

In this case, the wavefield reconstruction process becomes Equation X:

$$A\hat{u} = q + \lambda_{obs} \Sigma_{syn}^{-1} \hat{s} \tag{X}$$

The transformation significantly alleviates the computation memory problem, and the model gradient can be simplified into a straightforward form (**Equation XI**):

$$g = \left(\frac{\partial A}{\partial m}\right)^* \hat{u}(q, \hat{s})^* \hat{s} \tag{XI}$$

Next, we can divide the gradient into two terms by separating the wavefields excited by different sources q (d \hat{s}). The first term (**Equation XII**):

$$g_1 = \left(\frac{\partial A}{\partial m}\right)^* \hat{u}_0(q)^* \hat{s} \tag{XII}$$

Which is also the traditional FWI gradient, except for the blurred residual. The second term is (**Equation XIII**):

$$g_2 = \left(\frac{\partial A}{\partial m}\right)^* \hat{u}(\hat{s})^* \hat{s} \tag{XIII}$$

The above two terms are identical to the FWRI gradients developed in Lin *et al.*,³³ and its original **Equation XI** is directly derived from WRI, similar to the source extended FWI except for the source or data differences.

By comparison, we can see that the only difference between the data-domain and model-domain solutions is the extended source calculation, and the gradient calculation can be made through **Equations XII** and **XIII**.

2.4. The comparison between the two Hessian matrices

Here we write the two Hessian-based equations as follows (Equations XIV & XV):

$$\left[\lambda_{obs}(PA^{-1})\Sigma_{svn}(PA^{-1})^* + I\right]\delta d = \delta d^0 \tag{XIV}$$

$$[\lambda_{obs}(PA^{-1})^*(PA^{-1})\Sigma_{syn} + I]\hat{s} = s^0$$
 (XV)

Both equations are challenging to solve: **Equation XIV** involves a largeale matrix inverse calculation for the data residual, and **Equation IV** needs to operaten each wavefield or the extended source at each time step or frequency slice. A source-based definition of the theoretical covariance matrix has been proposed to alleviate the data-domain computation problem. Similarly, a proper definition of the theoretical covariance matrix should simplify the model-domain calculation problem.

Assuming the determinant of the first part of the model domain Hessian is significantly larger than the identity matrix, and all variables can be inverted, we have an approximated extended source expression (Equation XVI):

$$\hat{s} \approx \lambda_{obs}^{-1} \Sigma_{svn}^{-1} A P^{-1} P^{-*} A^* s^0$$
 (XVI)

Substituting the s^0 definition into **Equation XVI**, we have **Equation XVII**:

$$\hat{s} = \lambda_{obs}^{-1} \Sigma_{syn}^{-1} A P^{-1} P^{-*} A^* A^{-*} P^* \delta d^0 = \lambda_{obs}^{-1} \Sigma_{syn}^{-1} A P^{-1} \delta d^0$$
(XVII)

Notably, the derivation of the above equations relies on rough approximations and extreme assumptions. For the first part, the value of the first term of the Hessian, which is larger than the identity matrix, can be easily satisfied since it is a diagonal domain matrix and can be scaled by the theoretical matrix. We selected an exponential function, which can ensure this assumption. As for the second assumption, it essentially used the inverse of two operators.

One is the forward operator A, which is commonly used in inversion and imaging methods and applicable in the frequency codes. The other is the sampling operator P, which is mathematically incorrect to approximate the inverse of the adjoint $P^{-1} = P^*$.

However, the sampling operator is a dimensionality reduction operator that reduces the whole model space data to the receiver points, which is inevitable in seismic exploration. Therefore, one can only hope that the reduced data can recover the wavefield in the whole model space through the forward operator. In other words, the approximation of the sampling operator is mathematically incorrect but physically applicable. Although Equation XVII is similar to the extended source **Equation XI** in Huang et al., 18 the specific calculation is different: The SE-FWI method is a more accurate solution that requires additional calculation and storage of the Green function, while the proposed method in this paper is based on an approximation that only requires one additional partial differential equation (PDE) solver. In general, the extended source can be considered an operator on the receiver residual, where the operator is a function of the theoretical covariance matrix and the forward operator. The overall operator may help us to define the theoretical covariance matrix (Equation XVIII):

$$\hat{\Sigma}_{syn} = \Sigma_{syn}^{-1} A = \Sigma_{syn}^{-1} \left(m \frac{\partial^2}{\partial t^2} - L \right)$$
 (XVIII)

Where L is the Laplacian operator, the above equation reduces to a function in the receiver size due to the invertible assumption of the sampling operator P. Furthermore, the model-domain Hessian operates on each wavefield, while the original data comes from the source or receiver locations.

In general, through a series of approximations, assumptions, and derivations, we provide a straightforward method to define the theoretical covariance matrix, which ensures an accurate inversion with an affordable computational cost (**Equation XIX**):

$$\hat{\Sigma}_{syn} = \Sigma_{syn}^{-1} \left(x_r, x_r \right) \left[m \left(x_r \right) \frac{\partial^2}{\partial t^2} - L \left(x_r \right) \right]$$
 (XIX)

where x_r denotes the receiver locations.

Next, various theoretical covariance matrix definitions were given according to the inversion problem. Notably, through the above derivation, the calculation of the extended source was made simpler and more cost-effective (**Equation XX**), which is a simple operation for the original data residual at the receiver location.

$$\hat{s}(x_r,t) = \lambda_{obs}^{-1} \Sigma_{syn}^{-1}(x_r,x_r) \left[m(x_r) \frac{\partial^2}{\partial t^2} - L(x_r) \right]$$

$$\delta d^0(x_r,t)$$
(XX)

Various theoretical covariance matrix definitions are given and discussed in the following numerical test section. This part is only used for the wavefield reconstruction; the model gradient is calculated using **Equation VII**.

3. Numerical tests

3.1. Inversion test with smoothed initial model

In this section, we applied the proposed method to the classical Marmousi model. The size of the Marmousi model in Figure 1 is 250×767 with a 10 m space interval in each direction. A Ricker wavelet with 8 Hz central frequency with 2 Hz cutoff was used to simulate data in Figure 2. The recorded time was 3 s with a sampling of 1 ms. A total of 30 shots with 200 m intervals were set at a depth of 10 m beginning at 340 m, and the receivers were evenly distributed at a depth of 10 m at every grid point. The smoothed initial model is shown in Figure 3, which can be obtained by tomography or velocity analysis.

First, we presented the extended source used in WRI in Figure 4, where Figure 4A is the classical data residual used in the traditional WRI, and Figure 4B is the extended source calculated by **Equation XX**. We can see that the derived extended source exhibited a wider wavelength, making the misfit easier.

The final inversion results are shown in Figure 5, where Figure 5A is the traditional FWI result, Figure 5B plots the traditional WRI result, and Figure 5C is the WRI result based on the extended source (WRI-I). Due to the severely smoothed initial model, the traditional FWI failed to recover part of the key structures, especially in the deep parts. By comparison, the classical WRI provided a relatively accurate inversion result, where all structures were accurately located and inverted with limited artifacts. The WRI-I provided an accurate inversion result, where all the structures are recovered (especially the middle complex part) with fewer artifacts. Moreover, the computational cost of the new WRI is cheaper than that of the classical WRI. Both WRI results provided a more accurate inversion result at the deep part. For a clearer comparison, we extracted two traces from the true velocity and inversion results (Figure 6).

3.2. Inversion test with linear initial model

The basic parameters for the modeling and inversion were the same, except for the initial model, which is linear in Figure 7, causing more nonlinearity for the inversion. Furthermore, unlike other inversion tests, the initial

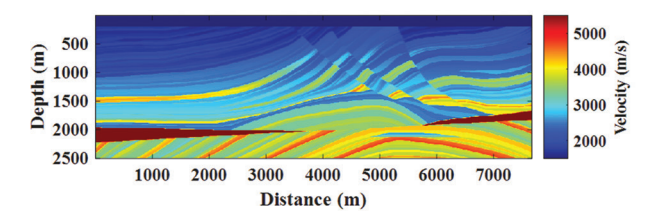


Figure 1. The Marmousi model

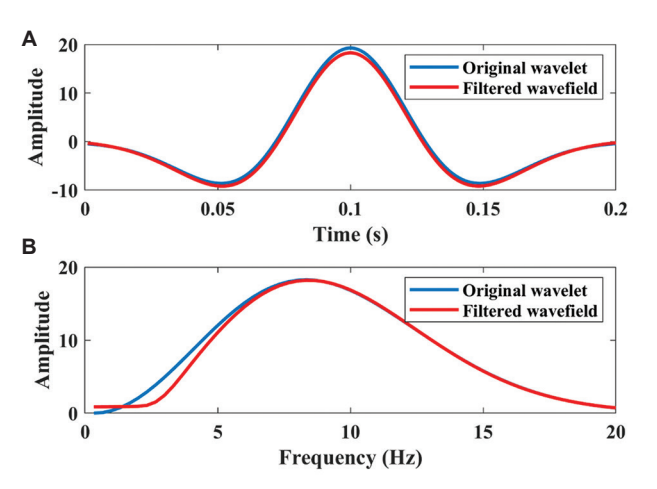


Figure 2. (A and B) Wavelet used for modeling and inversion

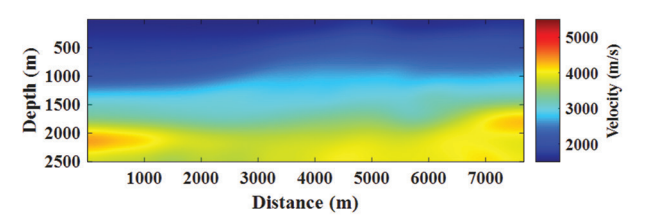


Figure 3. The smoothed Marmousi model

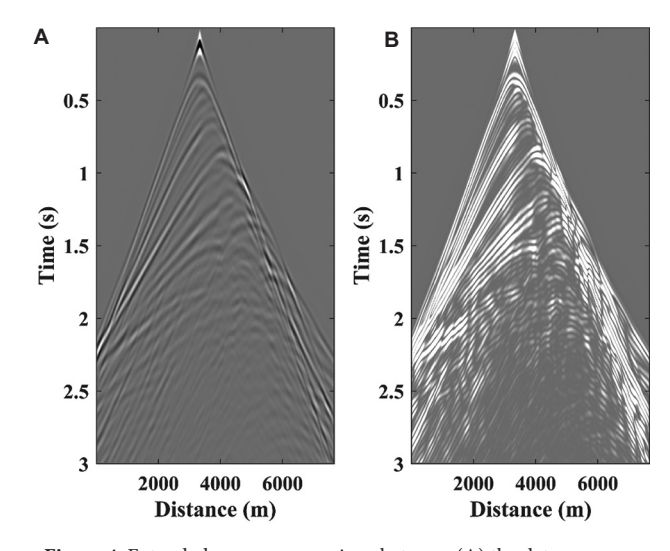


Figure 4. Extended source comparison between (A) the data resource calculated based on the identity matrix definition, and (B) the extended source calculated by **Equation XX**

Volume X Issue X (2025) 5 doi: 10.36922/JSE025250018

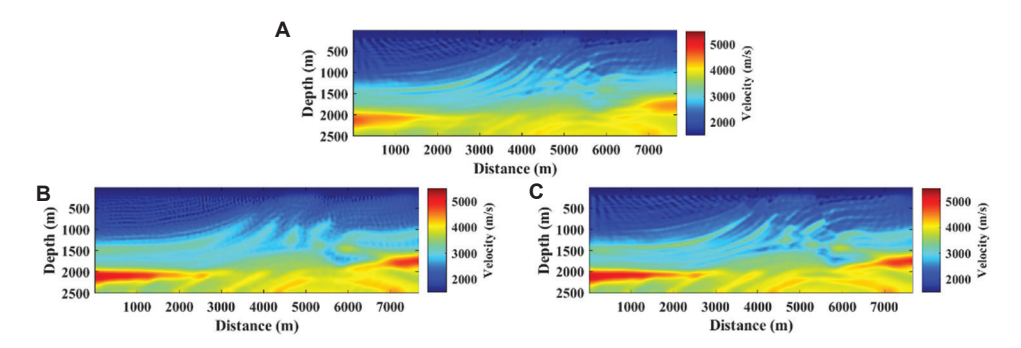


Figure 5. Inversion results. (A) Traditional full-waveform inversion result, (B) traditional wavefield reconstruction inversion (WRI) result, and (C) WRI result based on extended source.

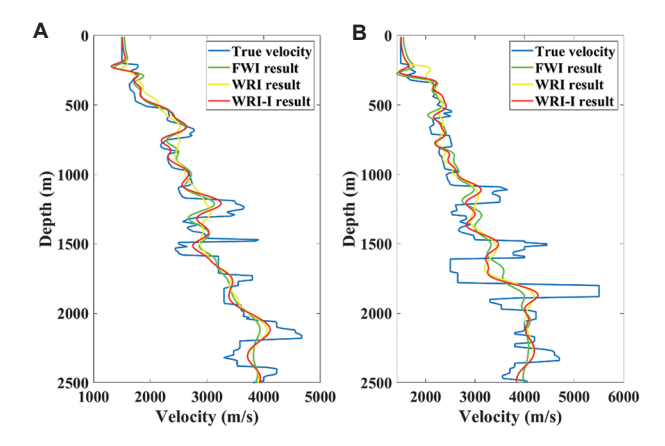


Figure 6. Comparison of vertical velocity profiles at different depths. (A) x = 3,800 m and (B) x = 6,500 m.

Abbreviations: FWI: Full waveform inversion: WPI: Wavefield

Abbreviations: FWI: Full-waveform inversion; WRI: Wavefield reconstruction inversion

model was significantly different from the true velocity, particularly in the deeper region. Therefore, we provided a new theoretical covariance matrix definition to aid the inversion (**Equation XXI**):

$$\sum_{syn} = exp^{-g(r)} \tag{XXI}$$

Where g is a manually picked function, and r denotes the distance between an arbitrary point and the source location: g(r) = 1/r. This equation is essentially an exponential function to emphasize the source distance, which is a known and relatively clear variable that can be used as an additional quantity for assistance in extended FWI or WRI.

Naturally, the extended sources used in WRI are shown in Figure 8, where Figure 8A is the classical data residual used in the traditional WRI, Figure 8B is the extended source calculated by Equation XX, and Figure 8C is the extended source calculated by Equation XXI. We can see that the data residual calculated by the newly defined theoretical covariance matrix is more structured

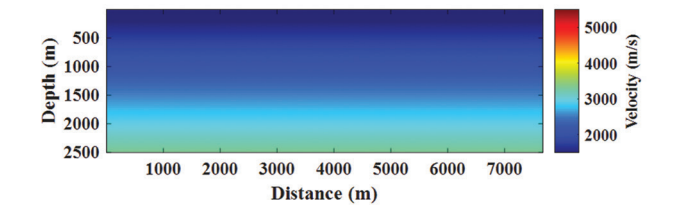


Figure 7. Linear initial model

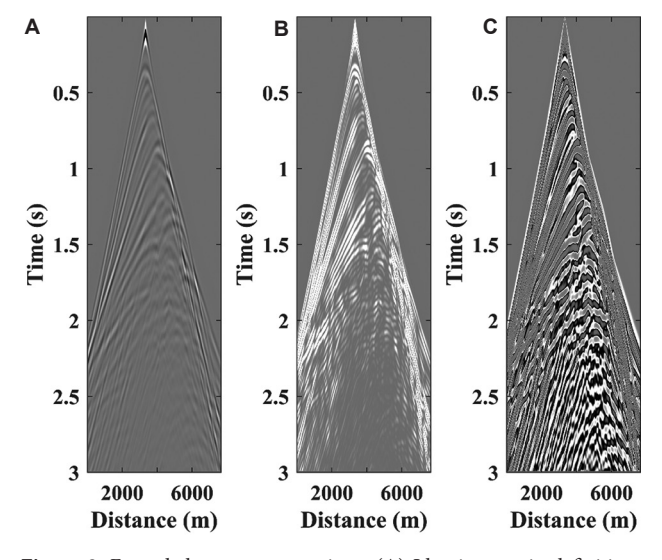


Figure 8. Extended source comparison. (A) Identity matrix definition, (B) calculated by **Equation XX**, and (C) calculated by **Equation XXI**.

at the waveform edges, and the deep reflections are more significant.

Due to the strong non-linearity caused by the initial model, the traditional FWI failed to perform an effective inversion and still showed no sign of convergence at the 50th iteration. The result (Figure 9A) contained many artifacts and was different from the true model. However, the traditional WRI (Figure 9B) produced an accurate inversion result, but with stronger artifacts that contaminated the shallow layers. Figure 9C plots the WRI-I,

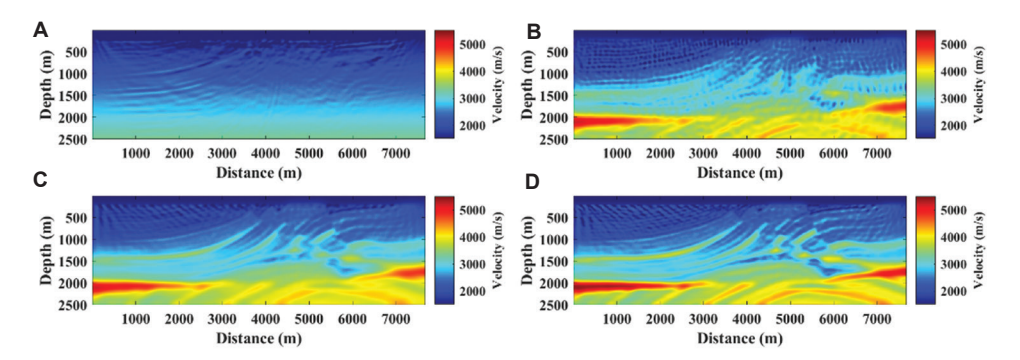


Figure 9. Inversion results. (A) Traditional FWI result, (B) traditional WRI result, (C) WRI result based on the extended source, and (D) WRI result based on the defined extended source.

Abbreviations: FWI: Full-waveform inversion; WRI: Wavefield reconstruction inversion.

and Figure 9D is the WRI-I calculated by Equation XXI. Both WRI methods based on the extended source yielded accurate inversion results. Meanwhile, the traditional one, that is, WRI-I, was still unable to obtain an accurate model in the middle. Furthermore, with a carefully defined theoretical covariance matrix, the WRI-I calculated by Equation XXI provided a very accurate inversion result that is very close to the true model without any evident artifacts. A curve comparison (Figure 10) is also provided to support the above claims.

Furthermore, a noisy test was conducted to highlight the robustness of the proposed method with respect to noise and to clarify the determination of the measurement constant. Figure 11 is the extended source used in WRI. An identity measurement covariance matrix can be used to describe random noise. Considering the role of the measurement constant λ_{obs} in the extended source equation and gradient formula, a subjectively determined constant that preserves modeling stability is sufficient, as was done in the previous tests. In the noise test, the constant was the same as the signal-to-noise ratio, which is estimated using the amplitude spectrum method.

As for the final inversion results (Figure 12), we observed that the noise in the extended source was entirely random and therefore did not form coherent wavefields capable of generating artifacts. However, the final results based on different theoretical covariance matrices showed slight deviations compared to the noise-free tests.

4. Discussion

The assumptions and approximations used in this study are generally applied in seismic inversion or imaging. For example, in most WRI methods, in which the penalty scalar is subjectively defined, the constant is commonly very large,²² which is consistent with our assumption that the main body of the model domain Hessian is larger than the identity matrix. Moreover, the sampling operator is also

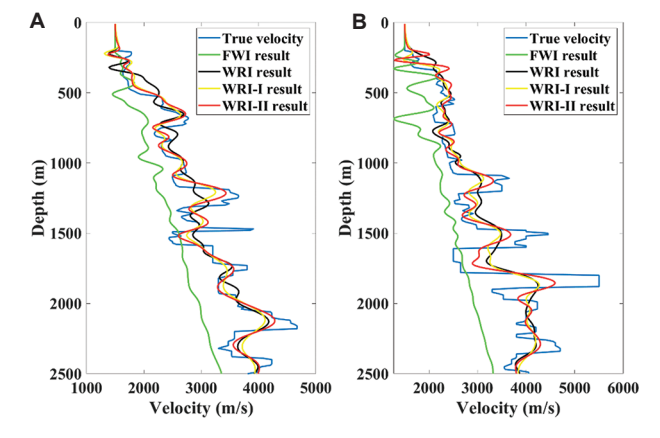


Figure 10. Trace comparison. (A) Located at x = 3,800 m, and (B) located at x = 6,500 m. Abbreviations: FWI: Full-waveform inversion; WRI: Wavefield reconstruction inversion.

defined subjectively, which can be the size of $N_{model} \times N_{receiver}$ or $N_{model} \times N_{model}$. Furthermore, **Equation XX** provided the final calculation method for the extended source used in this paper, ensuring the accuracy of the reconstructed wavefield. However, this series of approximations mainly focused on the computational time by transforming the space calculation to the receiver calculation, which weakens the potential of WRI in the model space, making it more applicable in complex cases with accurately calculated extended sources. Notably, the theoretical covariance matrix was defined before performing inversion, while most Bayesian-based inversion methods use the covariance matrix to evaluate the accuracy or resolution of the final results. The main difference between the two methods is the different definitions of the covariance matrix. In our method, the covariance matrix is separated into measurement and theoretical covariance matrices, representing different error distributions, respectively, while the other Bayesian-based method combines the two covariance matrices into one. However, according to the covariance matrix definition

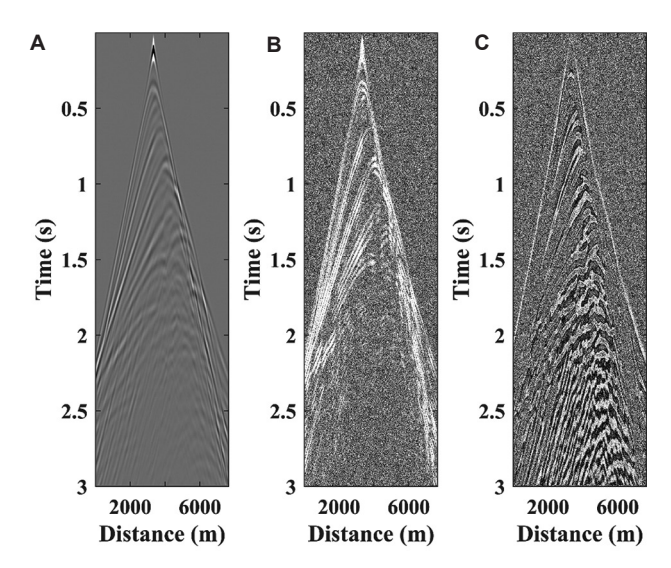


Figure 11. Extended source comparison. (A) Identity matrix definition, (B) calculated by **Equation XX**, and (C) calculated by **Equation (XXI)**.

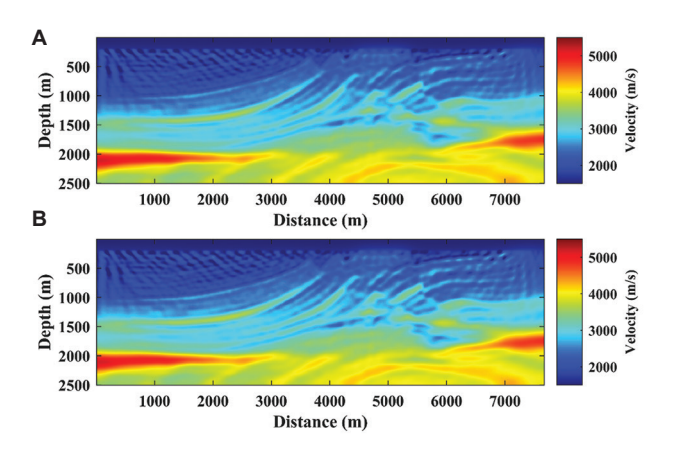


Figure 12. Inversion results. (A) Wavefield reconstruction inversion (WRI) result based on the extended source, and (B) WRI result based on the defined extended source.

in the Bayesian-based methods, the proposed method can be further evaluated based on the combined covariance matrix. Regarding the computational cost, the traditional WRI requires three PDE solvers, while the proposed method only requires two, similar to the traditional FWI. In addition, the source-extended FWI also needed three PDE solvers, the same as the fast WRI proposed by Lin *et al.*³³

5. Conclusion

This study introduced the Hessian, a function of the measurement and theoretical covariance matrices, into WRI based on Bayesian inference. Furthermore, the connections between the data and model domain equations were discussed, which led to a simplified extended source calculation method for the extended source. A theoretical covariance matrix definition based on the new calculation

method was proposed and validated through numerical tests. Further research may focus on more theoretical covariance matrix definitions and their effect on inversion.

Acknowledgments

None.

Funding

The study is supported by the Qingdao New Energy Shandong Laboratory Open Project under Grant QNESL OP202304.

Conflict of interest

Huaishan Liu is employed by the Key Laboratory of Oil & Gas Reservoir Geophysics, Sinopec, Beijing, China. The remaining authors declare they have no competing interests.

Author contributions

Conceptualization: Yuzhao Lin

Formal analysis: Yuzhao Lin, Huaishan Liu

Investigation: Huaishan Liu, Hehao Tang, Jinghao Li

Methodology: Huaishan Liu, Lei Xing Writing-original draft: Yuzhao Lin Writing-review & editing: Kun Huang

Availability of data

Data are available from the corresponding author on reasonable request.

References

 Tarantola A, Valette B. Generalized nonlinear inverse problems solved using the least squares criterion. Rev Geophys. 1982;20(2):219-232.

doi: 10.1029/RG020i002P00219

 Tarantola A. Inversion of seismic reflection data in the acoustic approximation. *Geophysics*. 1984;49(8):1259-1266.

doi: 10.1190/1.1441754

- 3. Tarantola A. *Inverse Problem Theory and Methods for Model Parameter Estimation*. Indian: SIAM; 2005.
- Virieux J, Operto S. An overview of full-waveform inversion in exploration geophysics. Geophysics. 2009;74(6): WCC1-WCC26.

doi: 10.1190/1.3238367

 Gauthier O, Virieux J, Tarantola A. Two-dimensional nonlinear inversion of seismic waveforms: Numerical results. *Geophysics*. 1986;51(7):1387-1403.

doi: 10.1190/1.1442188

6. Warner M, Guasch L. Adaptive waveform inversion: Theory.

Geophysics. 2016;81(6):R429-R445.

doi: 10.1190/geo2015-0387.1

7. Guasch L, Warner M, Ravaut C. Adaptive waveform inversion: Practice. *Geophysics*. 2019;84(1):R447-R461.

doi: 10.1190/geo2018-0377.1

8. Wu Z, Alkhalifah T. Selective data extension for full-waveform inversion: An efficient solution for cycle skipping. *Geophysics*. 2018;83(2):R201-R211.

doi: 10.1190/geo2016-0649.1

 Métivier L, Brossier R, Merigot Q, Oudet E, Virieux J. An optimal transport approach for seismic tomography: Application to 3D full waveform inversion. *Inverse Probl.* 2016;32(11):115008.

doi: 10.1088/0266-5611/32/11/115008

 Métivier L, Brossier R, Merigot Q, Oudet E, Virieux J. Measuring the misfit between seismograms using an optimal transport distance: Application to full waveform inversion. *Geophys J Int*. 2017;205(1):332-364.

doi: 10.1093/gji/ggw027

- Pladys A, Brossier R, Irnaka M, Kamath N, Métivier L. Graph Space Optimal Transport Based FWI: 3D OBC Valhall Case Study. SEG Tech Program Expanded Abstracts. United States: Society of Exploration Geophysicists; 2020. p. 696-700.
- Lin Y, Liu H, Sun J, Xing L. Time-domain wavefield reconstruction inversion based on unbalanced optimal transport. *IEEE Trans Geosci Remote Sens.* 2022;60:5920612. doi: 10.1109/TGRS.2022.3210576
- Bunks C, Saleck FM, Zaleski S, Chavent G. Multiscale seismic waveform inversion. *Geophysics*. 1995;60(5): 1457-1473.

doi: 10.1190/1.1443880

- 14. Fu L, Guo B, Schuster GT. Multiscale phase inversion of seismic data. *Geophysics*. 2018;83(3):R159-R171.
- 15. Symes WW. Objective Functions for Full Waveform Inversion. In: 74th EAGE Conference and Exhibition-Workshops; 2012.
- 16. Fu L, Symes WW. A discrepancy-based penalty method for extended waveform inversion. *Geophysics*. 2017;82(4):R287-R298.
- Fu L, Symes WW. An adaptive multiscale algorithm for efficient extended waveform inversion. *Geophysics*. 2017;82(3):R183-R197.

doi: 10.1190/geo2016-0426.1

18. Huang G, Nammour R, Symes WW. Full waveform inversion via source-receiver extension. *Geophysics*. 2017;82(3):R153-R171.

doi: 10.1190/geo2016-0301.1

 Huang G, Nammour R, Symes WW. Source-independent extended waveform inversion based on spacetime source extension: Frequency-domain implementation. *Geophysics*. 2018;83(5):R449-R461.

doi: 10.1190/geo2017-0333.1

20. Symes WW. Full Waveform Inversion by Source Extension: Why it Works. Preprint arXiv; 2020.

doi: 10.48550/arXiv.2003.12538

21. Leeuwen TV, Herrmann FJ. Mitigating local minima in full-waveform inversion by expanding the search space. *Geophys J Int.* 2013;195(1):661-667.

doi: 10.1093/gji/ggt277

 Leeuwen T, Herrmann FJ. A penalty method for PDEconstrained optimization in inverse problems. *Inverse Probl.* 2015;32(1):015007.

doi: 10.1088/0266-5611/32/1/015007

- Wang C, Yingst D, Farmer P, Leveille J. Full-Waveform Inversion with the Reconstructed Wavefield Method. In: Conference SEG Tech Program Expanded Abstracts; 2016. p. 1237-1241.
- Li ZC, Lin YZ, Zhang K, Li YY, Yu ZN. Time-domain wavefield reconstruction inversion. Appl Geophys. 2017;14(4):523-528.

doi: 10.1007/s11770-017-0629-6

- Rizzuti G, Louboutin M, Wang R, Daskalakis E, Herrmann F. A dual formulation for time-domain wavefield reconstruction inversion. In: SEG Tech Program Expanded Abstracts. United States: Georgia Institute of Technology; 2019. p. 1480-1485.
- 26. Rizzuti G, Louboutin M, Wang R, Herrmann F. A dual formulation of wavefield reconstruction inversion for large-scale seismic inversion. *Geophysics*. 2021;86(6):R879-R893.

doi: 10.1190/geo2020-0746.1

 Aghamiry HS, Gholami A, Operto S. Improving full waveform inversion by wavefield reconstruction with the alternating direction method of multipliers. *Geophysics*. 2019;84(1):R139-R162.

doi: 10.1190/geo2018-0093.1

28. Aghamiry HS, Gholami A, Operto S. Implementing bound constraints and total-variation regularization in extended full waveform inversion with the alternating direction method of multiplier: Application to large contrast media. *Geophys J Int.* 2019;212(2):855-872.

doi: 10.1093/gji/ggz189

 Aghamiry HS, Gholami A, Operto S. ADMM-based multi-parameter wavefield reconstruction inversion in VTI acoustic media with TV regularization. Geophys J Int. 2019:219(2):1316-1333.

doi: 10.1093/gji/ggz369

 Lin Y, Liu H, Xing L, Lin H. Time-domain wavefield reconstruction inversion solutions in the weighted full waveform inversion form. *IEEE Trans Geosci Remote Sens*. 2022;60(1):5923514.

doi: 10.1109/TGRS.2022.3224383

- Gholami A, Aghamiry HS, Operto S. Multiplier Waveform Inversion. Preprint arXiv; 2021.
- 32. Gholami A, Aghamiry HS, Operto S. Clarifying Some Issues on Extended FWI: Scattered-Field Equation, Time Reversal and Source Reconstruction. In: *Conference SEG Annual Meeting Expanded Abstracts*; 2021. p. 802-806.
- 33. Lin Y, Liu H, Xing L, Lin H. Time-domain wavefield reconstruction inversion solutions in the weighted full waveform inversion form. *IEEE Trans Geosci Remote Sens*. 2022;60(1):5923514.

doi: 10.1109/TGRS.2022.3224383

34. Operto S, Gholami A, Aghamiry HS, Guo G, Mamfoumbi F, Beller S. Full waveform inversion beyond the Born approximation: A tutorial review. *Geophysics*. 2023;88(6):WCC87-WC127.

doi: 10.1190/geo2022-0758.1

35. Stuart AM. Inverse problems: A Bayesian perspective. *Acta Numer*. 2010;19:451-559.

doi: 10.1017/S0962492910000031

36. Figueiredo LP, Grana D, Bordignon FL, Santos M, Roisenberg M, Rodrigues BB. Joint Bayesian inversion based on rock-physics prior modeling for the estimation of spatially correlated reservoir properties. *Geophysics*. 2018;83(1):M49-M61.

doi: 10.1190/geo2017-0363.1

37. Huang X, Eikrem KS, Jakobsen M, Nævdal G. Bayesian full-waveform inversion in anisotropic elastic media using the iterated extended Kalman filter. *Geophysics*. 2020;85(4):C125-C139.

doi: 10.1190/geo2019-0329.1

38. Leeuwen T. A Note on Extended Full Waveform Inversion. Preprint arXiv; 2019.

doi: 10.48550/arXiv.1904.00363

39. Lin Y, Leeuwen T, Liu H, Sun J, Xing L. A fast wavefield reconstruction inversion solution in the frequency domain. *Geophysics*. 2023;88(1):1-62.

doi: 10.1190/geo2022-0385.1

40. Gholami A, Aghamiry HS, Operto S. Extended Full Waveform Inversion in the Time Domain by the Augmented Lagrangian Method. arXiv Preprint; 2021.

doi: 10.48550/arXiv.2011.14102

41. Plessix RE. A review of the adjoint-state method for computing the gradient of a functional with geophysical applications. *Geophys J Int.* 2006;167(2):495-503.

doi: 10.1111/j.1365-246X.2006.02978.x